BULETINUL INSTITUTULUI POLITEHNIC DIN IAŞI
Publicat de
Universitatea Tehnică „Gheorghe Asachi” din Iaşi
Volumul 62 (66), Numărul 3, 2016
Secţia
MATEMATICĂ. MECANICĂ TEORETICĂ. FIZICĂ

INFLUENCE OF COMBUSTION AGENTS AND THERMAL TREATMENT ON PROPERTIES OF IRON MANGANESE OXIDES

BY

ELENA VASILICA GAFTON[1,*], GEORGIANA BULAI[1], IOAN DUMITRU[1], FLORIN TUDORACHE[1], OVIDIU F. CĂLȚUN[1], ADRIAN IULIAN BORHAN[2], ALEXANDRA RALUCA IORDAN[2] and MIRCEA NICOLAE PALAMARU[2]

“Alexandru Ioan Cuza” University of Iaşi,
[1]Faculty of Physics
[2]Faculty of Chemistry

Received: November 19, 2016
Accepted for publication: December 17, 2016

Abstract. Nanocrystalline iron manganese oxides with cubic structure were synthesized by autocombustion method using different fuel agents and annealing treatments. The synthesized samples were characterized by X-ray diffraction, vibrating sample magnetometry and electric measurements. The X-Ray analysis indicated that the phase content after combustion and in different stages of the thermal treatment is influenced by the type of fuel agent used in the synthesis process. The crystallite size of the obtained samples was found to be in nanoscale range. The specific saturation magnetization and the coercive field measurements confirmed the identification of the phase content. The permittivity and electrical resistivity measurements done on the powders obtained using hexamethylenetetramine, urea, and citric acid as combustion agents recommend the use of these samples for humidity sensor applications.

Keywords: nanostructures; sol-gel chemistry; X-ray diffraction; Rietveld analysis; humidity sensor.

[*]Corresponding author; *e-mail*: gafton.vasilica@gmail.com

1. Introduction

Polycrystalline oxides with general formula $A^{II}B^{III}O_3$, which have an inorganic chameleon due to the large flexibility of the structure (Hamdad, 2011) have drawn attention of researchers because of various applications. These materials can act as efficient heterogeneous catalysts (Watanabe *et al*., 2015) (Su *et al*., 2014), sensors (Ghasdi and Alamdari, 2010; Fergus, 2007), electrode materials for solid oxide fuel cells (Zhong *et al*., 2005) and gas storage (Xian *et al*., 2010; Chen *et al*., 2015).

Although $FeMnO_3$ properties were investigated by several research groups (Sfeir *et al*., 2005; Rayaprol *et al*., 2013; Seifu *et al*., 2000; Herranz *et al*., 2006; Leith *et al*., 1988), only a few applications have been reported. Li *et al*. studied electrochemical energy storage performances of supercapacitor based on $FeMnO_3$ hollow sphere/graphene composites. They reported that the obtained $FeMnO_3$ perovskite displays improved crystallization and different morphologies as the calcination temperature is increased (Li *et al*., 2014). Kulshreshtha *et al.* reported catalytic CO oxidation over γ-$FeMnO_3$ after palladium addition (Kulshreshtha *et al*., 2004). Rezlescu *et al*. prepared FeMnO3 perovskite by sol–gel self-combustion method and tested the samples for catalytic combustion of dilute acetone in air. The acetone conversion degree over perovskite catalysts exceeded 95% at 300°C (Rezlescu *et al*., 2015). Doroftei *et al*. studied the catalytic activity of the nanocrystalline $FeMnO_3$ for the combustion of acetone vapors and of some hydrocarbons diluted in air. The authors reported that the obtained perovskite is a good catalyst for gas and vapor combustion (Doroftei *et al*., 2014). Also, $FeMnO_3$ shows high capacity, excellent rate capability, and good cycling stability when used as electrode for Li batteries (Cao *et al*., 2016).

Our main objective was to synthesize pure nanocrystalline iron manganese oxide powders by sol-gel auto-combustion method and to investigate the influence of chelating/combustion agents on the structural features and magnetic properties by using, for the first time, five different chelating/combustion agents. As far as we know, no other papers reported the combined effect of different chelating/fuel agents on the structural, magnetic and sensing properties of $FeMnO_3$. The influence of different chelating/combustion agents on structural and physical properties of spinel oxides is related to their different interactions with the reactants, changing the morphology and crystallinity of the resulting powders (depending on the amount of generated heat) (Druc *et al.*, 2013). The effectiveness of magnetic materials used in sensor applications depends on the microstructural and magnetic properties of starting powders. The raw materials are very sensitive to the preparation conditions of sol-gel autocombustion method (Slatineanu *et al*., 2011). This method offers specific advantages in preparations of multi-component

oxide materials, such as: stoichiometric control of simple reactants, reduced synthesis time, good chemical homogeneity and nanometric size of the particles.

The novelty of this research consists in preparation of iron manganese oxide fine particles with various average size using different combustion agents for further application as humidity sensors. The particle size and phase content were controlled by changing the type of fuel agent which imposes different reaction speeds and temperatures. The influence of post annealing processes applied to achieve the desired phase was also studied. Detailed investigations of the structure and magnetic properties were done in order to understand the evolution from precursor solutions to the final powders.

2. Experimental Details

$FeMnO_3$ nanoparticles were prepared by sol-gel auto-combustion method. Analytical grade manganese nitrate, $[Mn(NO_3)_2 \cdot 4H_2O]$ (Aldrich) and iron nitrate (III), $[Fe(NO_3)_3 \cdot 9H_2O]$ (Aldrich) were mixed in stoichiometric proportions with different chelating/combustion agents such as: tartaric acid (99.9%, Aldrich) (AT), citric acid (99.9%, Merck) (AC), urea (99.9%, Merck) (U), glycine (99.9%, Merck) (Gly), and hexamethylenetetramine (99%, Merck) (Hex). Fig. 1 illustrates the reaction process that takes place during nanopowder synthesis. Reagents were dissolved in distilled water forming one solution for each chelating/combustion agent. Then fuel agents were added to each sample of metal nitrates mixture in 1:1 molar ratio of fuel agent: metallic cations. After synthesis step, the solutions were heated at 75ºC through gel phase transformation and then naturally cooled down to room temperature to obtain dry gel. The gels were gradually heated at 300ºC, during which autocombustion occurred (Slatineanu *et al.*, 2011). The samples were labelled as MF_AT, MF_AC, MF_U, MF_Gly and MF_Hex.

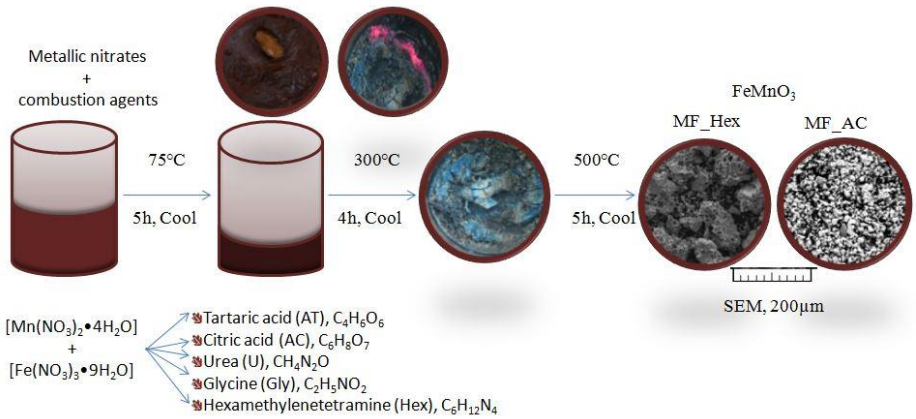

Fig. 1 − An illustrated sol-gel combustion method process for the synthesis of $FeMnO_3$.

To understand the process dynamics, the as-synthesized powders were micro-structurally and magnetically characterized. After a first phase content analysis of the powders annealed at 500ºC for 5 h a subsequent thermal treatment was done at 900°C for 7h. Part of as-synthesized powders was directly calcined at 1200°C for 4h in air. The phase content and magnetic properties were checked at every synthesis step. X-ray diffraction (XRD) was performed using a Shimadzu LabX XRD-6000 (Cu *Kα* radiation, λ = 1.5405 Å) with 2θ ranging between 20° and 90° and 0.02° scanning rate. Magnetic measurements were performed at room temperature using a vibrating sample magnetometer system (Model VSM 3900 Princeton). Electrical properties were studied using an Agilent E4980A Precision LCR Meter-type impedance analyzer. Permittivity and electrical resistivity measurements, in the frequency range of 20 Hz - 107 Hz, were performed in parallel-plate capacitor configuration, by applying Pd − Ag electrodes on the polished surfaces of the $FeMnO_3$ disks (6 mm diameter, 2 mm thickness) obtained by pressing. The influence of humidity on the electrical properties was analyzed by placing the samples into a closed box at 23°C with controlled humidity between 0% and 100% RH.

3. Results and Discussion

3.1. Structural Analysis

The XRD patterns of the iron manganese oxides calcined at 500°C are shown in Fig. 2*a*. All the identified peaks were indexed in good agreement with the referred ICDD cards (* * ICDD). The results revealed the presence of α-Fe_2O_3 (antiferromagnetic) and $FeMnO_3$ (ferrimagnetic) phases in different ratios. Phases content for each sample and lattice parameters determined from Rietveld analysis are reported in Table 1. One can observe that the combustion agent has a significant influence on α-Fe_2O_3 phase content which varies from 20.89% in MF_Hex to 94.2% in MF_U.

A further thermal treatment of the powders at higher temperature was performed at 900°C. As one can observe from the diffraction patterns presented in Fig. 2*b*, the α-Fe_2O_3 phase increases, but a small amount of $FeMnO_3$ still exist. Phase content analysis of samples calcined directly at 1200°C demonstrated that high temperatures favor the formation of $FeMnO_3$ (ferrimagnetic structure at room temperature) accompanied by a low percentage of $MnFe_2O_4$ (ferrimagnetic spinel structure). The highest ratio of spinel phase content of 4% corresponds to MF_U sample.

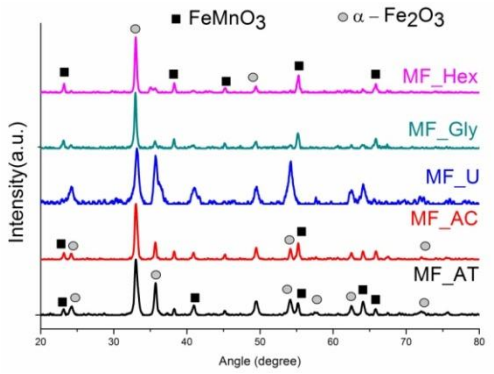

a

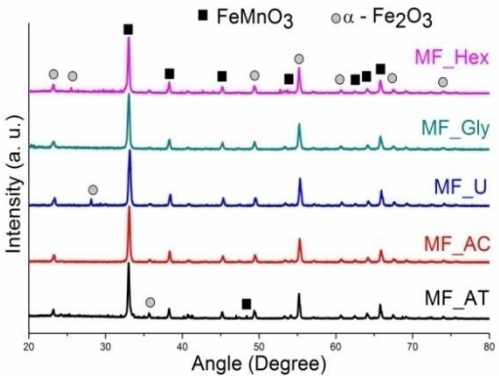

b

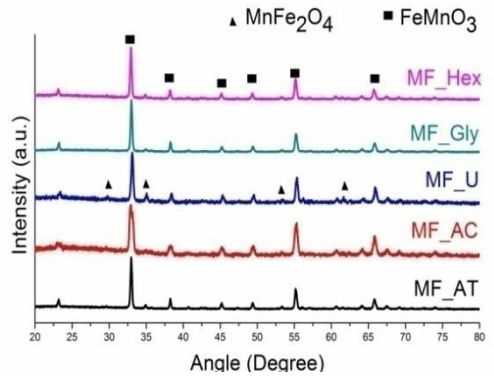

c

Fig. 2 − XRD patterns (color online) of iron manganese oxides powders synthesized with different agents and annealed at different temperatures: *a*) 500°C, *b*) 900°C and *c*) 1200°C.

Table 1
Phase Content of Samples Annealed at Different Temperatures. GofF Represents the Goodness of Fit

	°C	$MnFe_2O_4$		α-Fe_2O_3			$FeMnO_3$		GofF
		%	a	%	a	c	%	a	
MF_AT	500			71.56	5.03(2)	13.7596(3)	28.44	9.4057(1)	1.09
	900			15.73	5.3089(6)	13.4737(3)	84.27	9.4175(9)	1.82
	1200	1.41	8.5266(5)				98.59	9.4139(1)	1.45
MF_AC	500			44.9	5.0336(4)	13.4734(5)	55.1	9.408(7)	1.06
	900			6.65	5.3068(1)	13.7453(7)	93.35	9.4119(7)	1.34
	1200	0.31	8.6378(6)				99.69	9.4073(5)	1.62
MF_U	500			94.2	5.9267(5)	13.7754(4)	5.8	9.6082(9)	1.17
	900			4.34	5.0419(1)	13.7609(8)	95.66	9.4166(7)	1.54
	1200	4.03	8.5343(6)				95.97	9.4212(9)	1.38
MF_Gly	500			35.3	5.0293	13.775(2)	64.7	9.4057(1)	1.1
	900			1.02	5.0344(7)	13.7945(3)	98.98	9.4142(5)	1.36
	1200	0.44	8.1595				99.56	9.4131(3)	1.47
MF_Hex	500			20.89	5.0475(6)	13.72	76.36	9.4024(8)	1.17
	900			3.46	5.3094	13.7558(5)	96.54	9.1347(5)	1.76
	1200	1.85	8.5257(1)				98.15	9.4138(6)	1.39

The broad XRD lines indicate that crystallites are in nanosize scale. The crystallite sizes listed in Table 2 were calculated from 222 peak broadening found at $2\theta \approx 33°$ using Debye-Scherrer formula: $D = \frac{0.89 \cdot \lambda}{\beta \cdot \cos\theta}$, where D is the crystallite size, λ is the wavelength of X-ray used, β (rad) is the full width at half maximum of the diffraction peak and θ is the diffraction angle. The highest value of 41 nm was observed for MF_AT sample calcined at 900°C.

Table 2
Crystallites Size in Nanometers of $FeMnO_3$ Powders Thermally Treated from X-ray Diffraction Patterns

$FeMnO_3$	AT	AC	U	Gly	Hex
500°C	18	21	15	28	27
900°C	41	34	28	29	35
1200°C	36	15	29	35	35

The average crystallite size is strongly influenced by the intensity of the combustion reaction. Combustion induced by tartaric acid is the less intense (Dumitrescu *et al*., 2013) and it explains the larger crystallite size than in the

other cases. Usually, high annealing temperature increases the particle size due to Oswald ripening (Zeng, 2007).

3.2. Magnetic Properties

Magnetizations (M) *versus* magnetic field (H) hysteresis loop measured at room temperature are presented in Fig. 3 and the values of the magnetic parameters are listed in Table 3. Magnetic properties of nanoparticles are influenced by the phase content and average particles size. The shape of the curves for the powders calcined at 500°C and synthesized using hexamethylenetetramine and citric acid as combustion agents have higher magnetization values, which can be explained by the higher $FeMnO_3$ phase percentage determined from XRD patterns.

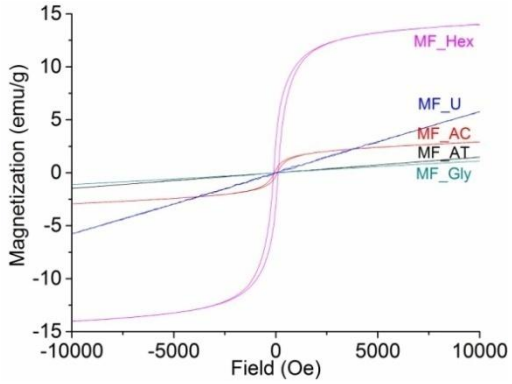

a

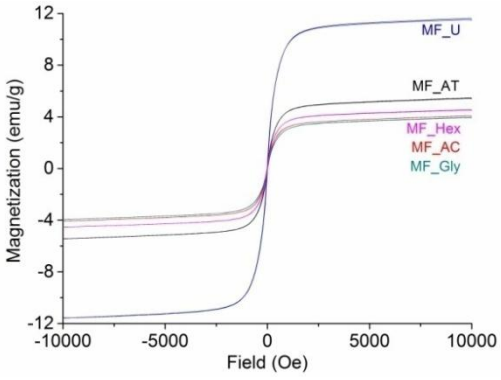

b

Fig. 3 – Magnetization as a function of applied field loops of $FeMnO_3$ powders sintered at: *a*) 500°C and *b*) 1200°C.

For powders corresponding to same annealing temperatures, the higher magnetization is due to the higher percentage of the magnetic phase. The use of different fuel agents influences the geometrical arrangement of the different cations and the resulting magnetic coupling.

Table 3
Magnetic Parameters of $FeMnO_3$ Powders

$FeMnO_3$	M_S (emu/g)		H_C (Oe)	
	500°C	1200°C	500°C	1200°C
MF_AT	0.4	5.4	--	11
MF_AC	0.7	4.1	70	14
MFU	0.3	11.1	--	12
MF_Gly	2	3.9	--	20
MF_Hex	9	4.4	109	15

MF_Hex powder calcined at 500°C, with D_{cryst} = 27 nm, exhibits the largest values of coercivity, 109 Oe, and specific magnetization, 10.7 emu/g. The powders prepared with urea and tartaric acid appears to be paramagnetic at room temperature, observation that can be correlated to the large ratio of α-Fe_2O_3 identified in XRD patterns. The values of saturation magnetization for the powders thermally treated at 1200°C are generally higher compared with the samples calcined at 500°C. These values ranging between 4 and 11 emu/g correspond to the $FeMnO_3$ phase and are comparable with ones reported in literature (Rayaprol *et al*., 2013). For example, in case of MF_U, a crystalline $FeMnO_3$ and $MnFe_2O_4$ phase was formed at 1200°C, leading to a magnetization increase to 10 emu/g. In addition, a small increase in the magnetic properties can be attributed to the increase in crystallite size for all materials from 15 nm at 500°C to 36 nm at 1200°C. This behavior indicates a direct relationship between magnetic properties and crystal growth as observed by Zhang *et al*. in their study on $MnFe_2O_4$ obtained by coprecipitation (Zhang and Nan, 2015).

3.3. Electrical Properties under Humidity Influence

In order to use the materials as humidity sensors, their electrical properties are relevant. The relative permittivity and electrical resistivity are mainly dependent on the ion exchange mechanism between ions from different positions, corresponding to typical cubic structures. As shown in Figs. 4 and 5, the relative permittivity and electrical resistivity of all samples decrease with the frequency in the relative humidity range 0–100% RH, in accordance with typically Maxwell–Wagner type interfacial polarization (Jawada *et al*., 2012).

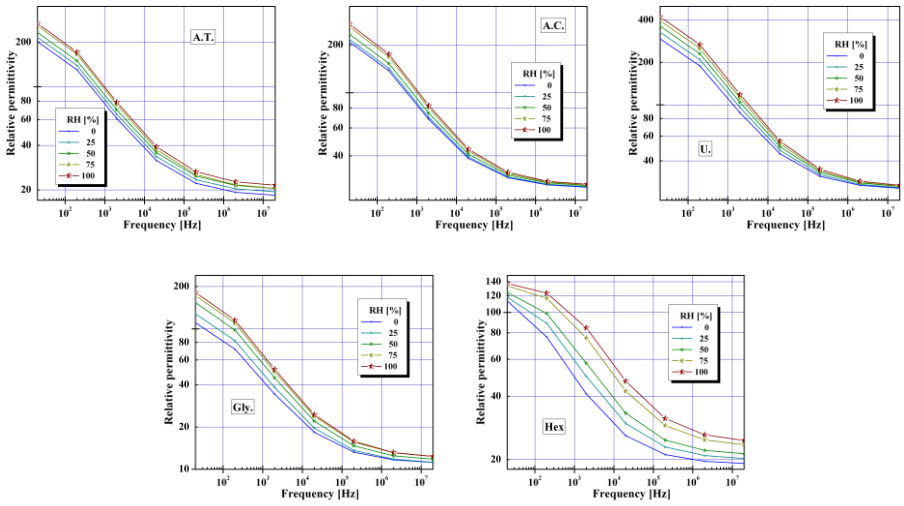

Fig. 4 – Frequency dependence of the relative permittivity at room temperature in the relative humidity range 0–100%.

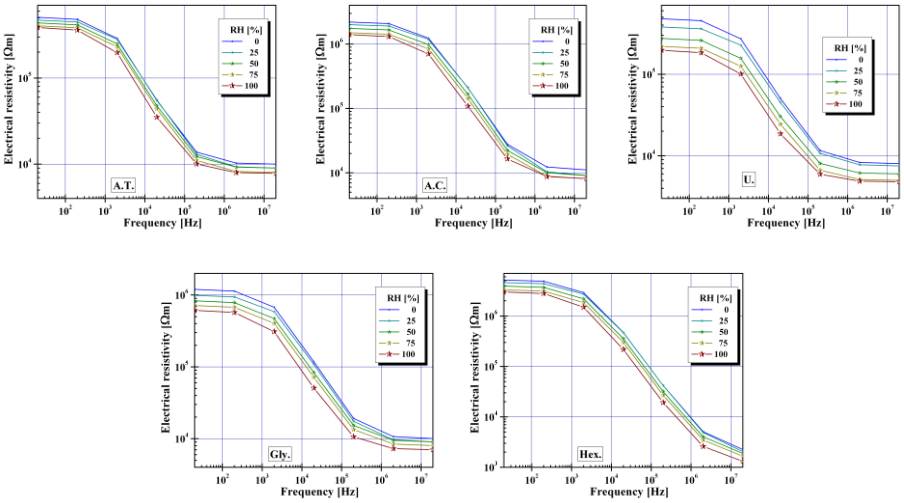

Fig. 5 – Variation of electrical resistivity with frequency in presence of water vapors.

According to this theory, the conductivity of grain boundaries contributes more to the relative permittivity at lower frequencies. Normally, with increasing of annealing temperature, there is an increase of relative permittivity and a decrease of electrical resistivity due to the formation of grains

with high conductivity (Petrila and Tudorache, 2013). Therefore, we have investigated the electrical properties of the cubic type oxides annealed at 900°C, because the high values of electrical resistivity hinder the use as materials for humidity sensors, although its sensitivity to humidity is high. The difference between the values of electrical resistivity indicates that the use of urea as fuel agent is favorable. Instead, the use of the hexamethylenetetramine (Hex) as chelating/combustion agent lead to the formation of secondary phases which occur due to short combustion time and high temperature during combustion (Druc *et al*., 2013). However, the resistivity of all materials prepared is brought into the measurable zone, useful for sensors applications.

At 20 Hz, the relative permittivity values of MF_U and MF_Hex samples at 100% relative humidity are 400 and 140, respectively. The rest of materials have the permittivity almost equal to 200. The variation of permittivity response depending on the frequency is strongly influenced by the crystallinity, porosity, grain size, and pore-size distribution within the microstructure (Muthu and Lakshminarasimhan, 2013). Hence, this variation can be attributed to the structural changes caused by fuel agents. The humidity, as expected, produces an increase in permittivity and a decrease in resistivity of the materials, because of open pores filling with water vapors. It can be observed that for low relative humidity, all samples possess high electrical resistivity values, which decreases with increasing of RH, [%]. Therefore, the humidity influence on the relative permittivity and electrical resistivity function of frequency can be attributed to the Maxwell–Wagner Debye relaxation in the case of the vapors that fill the materials pores (Tudorache *et al*., 2013) However, it is interesting that for MF_U was obtained the lowest value of electrical resistivity. This could be related to the long time of the auto-combustion process, allowing stabilization of the structure. Another reason could be the occupation of the lattice positions by the ions. The results indicate large variations of permittivity and electrical resistivity under humidity of prepared samples, and recommend that these materials can be used as humidity sensors. In this respect, the sensitivity to humidity can be highlighted by the capacitive or resistive humidity sensitivity coefficients. In Fig. 6(*a*-*b*) the capacitive and resistive humidity sensitivity coefficients of sensors in function of relative humidity based on iron manganese oxides are represented. As can be seen, the sensitivity of both resistive and capacitive sensors is increased with increase of the temperature treatment mainly due to the microstructure and pore size distribution. All the sensors exhibit S_R smaller than 60%, and started to respond for extremely low RH values (of about 2%). It is worth to note that the device based on MF_U oxide showed higher S_R (about 58%), but the onset for all materials did not change.

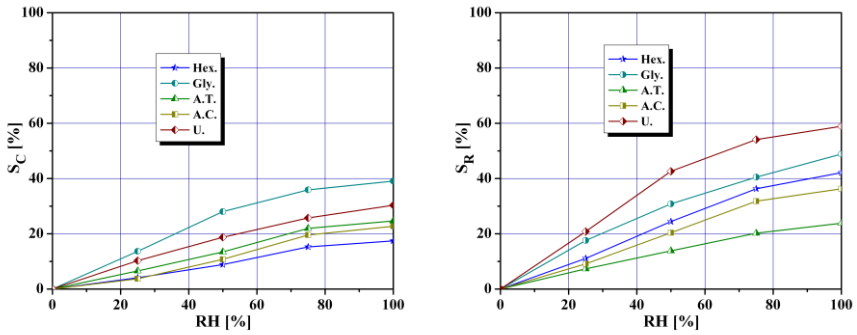

a *b*

Fig. 6 – Humidity sensitivity characteristics of iron manganese material: *a*) Capacitive humidity sensitivity dependence on relative humidity; *b*) Resistive humidity sensitivity dependence on relative humidity.

According to literature, the chemisorption in oxides can be discarded at higher humidity levels, while physical adsorption takes place in the whole range of relative humidity and the time required to reach equilibrium is the time necessary for the H_2O pressure to establish into the various parts of the materials (Cavalieri *et al*., 2012). At room temperature, the resistance humidity coefficient is mainly determined by the grain boundary resistance of the MF oxides. Taking this into account, the mechanism could consist in water adsorption, when a few water vapors tend to chemically adsorb on the grain surfaces of the oxide oxides giving rise to M–OH hydroxyl groups (Jing-Li *et al*., 1991). Then, if more water vapor is adsorbed, liquid-like multilayer of hydrogen-bonded water molecules is formed, which condense into mesopores. Therefore, the dominant charge carriers in the water adsorbed in the mesopores are H^+ protons, which increase with increasing the moisture content. Protons H^+ can move freely in liquid water, giving a decrease of grain surface resistance with increasing relative humidity RH. This mechanism explains why electrical resistivity decreases with increasing relative humidity RH, leading to an increase of sensitive response S_R (Viviani *et al*., 2001). In contrast to the resistive coefficient, the capacitive increases with increasing relative humidity RH, because the capacitance reflects the dielectric property of the MF oxides. Since water vapor molecules can be highly polarized, the accumulation of water on the grain surface of the MF samples increases the dielectric coefficient of the sensors.

3. Conclusions

Iron manganese oxides powders were synthesized by autocombustion method using five different combustion agents. The combustion fuels strongly influenced the phase composition. The $FeMnO_3$ percentage varied from 6% (for

MFU) to 76% (for MF_Hex) in the case of the powders calcined at 500°C. As a result the magnetic behavior changed from a paramagnetic state (MFU and MF_AT) to a ferrimagnetic one (MF_Hex and MF_AC). For the powders calcined at 1200°C the main observed phase was a ferrimagnetic oxide accompanied by small percentages of manganese ferrite. The highest saturation magnetization value of 11 emu/g was observed for MFU sample which also presented the highest percentage of manganese ferrite phase. MF perovskites exhibit large variations of permittivity and electrical resistivity under humidity influence, suggesting possible application as humidity sensors.

Acknowledgements. I. Dumitru acknowledges the support given by Romanian CNCS-UEFISCDI, project number PN-II-RU-TE-2012-3-0449.

REFERENCES

Cao K. *et al*., *$FeMnO_3$: a High-Performance Li-Ion Battery Anode Material*, Chem. Commun., Vol. **52**, 11414-11417 (2016).

Cavalieri A. *et al*., *Electrical Characterization of Room Temperature Humidity Sensors in $La_{0.8}Sr_{0.2}Fe_{1-x}Cu_xO_3$ (x = 0, 0.05, 0.10)*, Ceram. Int., Vol. **38**, 2865-2872 (2012).

Chen C.-F. *et al*., *Oxygen-Deficient $BaTiO_{3-x}$ Perovskite as an Efficient Bifunctional Oxygen Electrocatalyst*, Nano Energy, Vol. **13**, 423-432 (2015).

Doroftei C. *et al*., *Structural and Catalytic Characterization of Nanostructured Iron Manganite* , Composites Part. B, Vol. **67**, 179-182 (2014).

Druc A.C. *et al*., *Optimization of Synthesis Conditions and the Study of Magnetic and Dielectric Properties for MgFe2O4 Ferrite*, Cent. Eur. J. Chem., Vol. **11**, *8*, 1330-1342 (2013).

Dumitrescu A.M. *et al*., *Study of the Chelating/Fuel Agents Influence on $NiFe_2O_4$ Samples with Potential Catalytic Properties*, Powder Technology, Vol. **243**, 9-17 (2013).

Fergus J.W., *Perovskite Oxides for Semiconductor-Based Gas Sensors*, Sens. Actuators, Vol. **B 123**, 1169-1179 (2007).

Ghasdi M., Alamdari H., *CO Sensitive Nanocrystalline $LaCoO_3$ Perovskite Sensor Prepared by High Energy Ball Milling*, Sens. Actuators, Vol. **B 148**, 478-485 (2010).

Hamdad N., *The Ground States Properties and the Spin Effect on the Cubic and Hexagonal Perovskite Manganese Oxide $BaMnO_3$: GGA+U Calculation*, Physica B, Vol. **406**, 1194-1203 (2011).

Herranz T. *et al*., *Synthesis, Structural Features, and Reactivity of Fe−Mn Mixed Oxides Prepared by Microemulsion*, Chem. Mater., Vol. **18**, *9* (2006).

Leith I.R., Howden M.G. *Temperature-Programmed Reduction of Mixed Iron-Manganese Oxide Catalysts in Hydrogen and Carbon Monoxide*, Appl. Catal. A-Gen., Vol. **37**, 75-92 (1988).

Jawada A.S. *et al*., *Exploring the Dielectric Behaviour of Nano- Structured Al^{3+} Doped $BiFeO_3$ Ceramics Synthesized by Auto Ignition Process*, J. Alloys Compd., Vol. **530**, *25*, 63-70 (2012).

Jing-Li Z. *et al*., *Electrical Conduction of $La_{1-x}Sr_xFeO_3$, Ceramics under Different Relative Humidities*, Sens. Actuators A: Phys., Vol. **29**, 43-47 (1991).

Kulshreshtha S.K. *et al*., *CO Oxidation Over Pd/ -$FeMnO_3$ Catalyst*, Indian J. Chem. Technol., Vol. **11**, 427-433 (2004).

Li M. *et al*., *Facile Synthesis of Specific $FeMnO_3$ Hollow Sphere/Graphene Composites and their Superior Electrochemical Energy Storage Performances for Supercapacitor*, J. Power Sources, Vol. **248**, 465-473 (2014).

Muthu K.S., Lakshminarasimhan N., *Impedance Spectroscopic Studies on $NiFe_2O_4$ with Different Morphologies: Microstructure vs. Dielectric Properties*, Ceram. Int., Vol. **39**, 2309-2315 (2013).

Petrila I., Tudorache F., *Humidity Sensor Applicative Material Based on Copper-Zinc-Tungsten Spinel Ferrite*, Mater. Lett., Vol. **108**, 129-133 (2013).

Rayaprol S. *et al*., *Structure and Magnetism of $FeMnO_3$*, AIP Conf. Proc., Vol. **1512**, 1132 (2013).

Rayaprol S. *et al*., *Structure and Magnetism of $FeMnO_{3n}$*, Proceedings of the 57th Dae Solid State Physics Symposium 2012, Solid State Physics, AIP Publishing, 2013, Vol. **1512**.

Rezlescu N. *et al*., *Some Nanograined Ferrites and Perovskites for Catalytic Combustion of Acetone at Low Temperature*, Ceram. Int., Vol. **41**, 4430-4437 (2015).

Seifu D. *et al*., *Evidence of Ferrimagnetic Ordering in $FeMnO_3$ Produced by Mechanical Alloying*, J. Magn. Magn. Mater., Vol. **212**, 1-2 (2000).

Sfeir J. *et al*., *Characterization of Perovskite Powders for Cathode and Oxygen Membranes Made by Different Synthesis Routes*, J. Eur. Ceram. Soc., Vol. **25**, 1991-1995 (2005).

Slatineanu T. *et al*., *Synthesis and Characterization of Nanocrystalline Zn Ferrites Substituted with Ni*, Mater. Res. Bull., Vol. **46**, *9*, 1455-1460 (2011).

Su Y.J., Pan K.L., Chang M.-B., *Modifying Perovskite-Type Oxide Catalyst LaNiO3 with Ce for Carbon Dioxide Reforming of Methane*, Int. J. Hydrogen Energy, Vol. **39**, 4917-4925 (2014).

Tudorache F. *et al*., *Influence of Thermal Treatment on the Structure, Humidity Sensitivity, Electrical and Magnetic Properties of Barium–Tungsten Ferrite*, Compos. Part B, Vol. **51**, 106-111 (2013).

Viviani M. *et al*., *Barium Perovskites as Humidity Sensing Materials*, J. Eur. Ceram. Soc., Vol. **21**, 1981-1984 (2001).

Watanabe R., Saito Y., Fukuhara C., *Enhancement of Ethylbenzene Dehydrogenation of Perovskite-Type $BaZrO_3$ Catalyst by a Small Amount of Fe Substitution in the B-Site*, J. Mol. Catal. A: Chem., Vol. **404**, 57-64 (2015).

Xian H. *et al*., *Effect of the Calcination Conditions on the NO_x Storage Behavior of the Perovskite $BaFeO_{3-x}$ Catalysts*, Catal. Today, Vol. **158**, 215-219 (2010).

Zeng H.C., *Ostwald Ripening: A Synthetic Approach for Hollow Nanomaterials*, Curr. Nanosci., Vol. **3**, 177-181 (2007).

Zhang Y., Nan Z., *Modified Magnetic Properties of $MnFe_2O_4$ by CTAB with Coprecipitation Method*, Mater. Lett., Vol. **149**, 22-24 (2015).

Zhong G.Q., Xiong H., Jia Y.Q., *Synthesis, Crystal Structure, Relative Content of the Mn^{4+} Ion, Tolerance Factor and Catalytic Property of $La_{1-x}Ca_xMnO_3$* (x= 0.0–1.0), Mater. Chem. Phys., Vol. **91**, 10-16 (2005).

$^{*}_{*}{}_{*}$ ICDD FeMnO3-ICDD 75-0894, Fe2O3 – ICDD 89-2810.

INFLUENȚA AGENȚILOR DE COMBUSTIE ŞI A TRATAMENTELOR TERMICE ASUPRA PROPRIETĂȚILOR OXIZILOR FERICI DE MANGAN

(Rezumat)

Nanoparticule de oxizi ferici de mangan cu structură spinelică au fost sintetizate prin metoda solgel utilizând diferiți agenți de combustie și supuse ulterior unei serii de tratamente termice. Eşantioanele au fost caracterizate din punct de vedere structural, magnetic şi electric. Măsurătorile magnetice au fost realizate la temperatura camerei prin intermediul unui sistem magnetometric cu probă vibrantă. Analizele de difractometrie au indicat că conținutul de fază după combustie și în diferite etape ale tratamentului termic este influențat de agentul de combustie folosit în procesul de sinteză. Dimensiunea cristalitelor eșantioanelor obținute este în domeniul nanometric. Măsurătorile magnetizației de saturație specifică și a câmpurilor coercitive au confirmat identificarea conținutului de fază. Măsurătorile permitivității și rezistivității electrice realizate pe eșantioanele conținând hexametilentetramină, uree și acid citric recomandă utilizarea acestora ca materiale de bază în confecționarea senzorilor.